Hybrid Modeling, Identification, and Predictive Control: An Application to Hybrid Electric Vehicle Energy Management

G. Ripaccioli[1], A. Bemporad[1], F. Assadian[2], C. Dextreit[2], S. Di Cairano[3], and I.V. Kolmanovsky[3]

[1] Dept. of Information Engineering, University of Siena, Italy
{ripaccioli,bemporad}@dii.unisi.it
[2] Jaguar Land Rover Research
{fassadia,cdextrei}@jaguarlandrover.com
[3] Ford Motor Company, Dearborn, Michigan, USA
{sdicaira,ikolmano}@ford.com

Abstract. Rising fuel prices and tightening emission regulations have resulted in an increasing need for advanced powertrain systems and systematic model-based control approaches. Along these lines, this paper illustrates the use of hybrid modeling and model predictive control for a vehicle equipped with an advanced hybrid powertrain. Starting from an existing high fidelity nonlinear simulation model based on experimental data, the hybrid dynamical model is developed through the use of linear and piecewise affine identification methods. Based on the resulting hybrid dynamical model, a hybrid MPC controller is tuned and its effectiveness is demonstrated through closed-loop simulations with the high-fidelity nonlinear model.

Keywords: Hybrid systems, model predictive control, powertrain control, hybrid electric vehicles, piecewise affine systems, piecewise affine system identification.

1 Introduction

The complexity of powertrain systems is increasing in response to tightening fuel economy and emission requirements. In particular, the powertrains have now more subsystems, components, inputs, outputs, operating modes and constraints than in the past. Their effective treatment benefits from systematic modeling and model-based control approaches.

In the paper we demonstrate how a hybrid dynamical model of an advanced powertrain can be developed using linear and piecewise affine identification techniques. The resulting hybrid model can be used as a basis for the design of a hybrid Model Predictive Controller which uses mixed integer quadratic programming (MIQP) solvers for the on-line optimization to coordinate commands to powertrain subsystems and enforce pointwise-in-time state and control constraints.

R. Majumdar and P. Tabuada (Eds.): HSCC 2009, LNCS 5469, pp. 321–335, 2009.

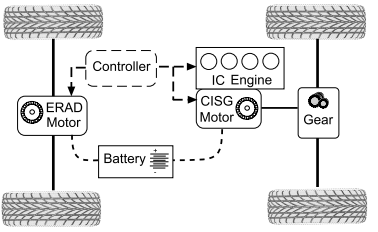

Fig. 1. Configuration of the 4x4 hybrid electric vehicle

A specific case study based on a parallel Hybrid Electric Vehicle (HEV) introduced in [1] has been chosen to demonstrate the proposed approach. This vehicle relies on two electric motors (one in the front and one in the rear of the vehicle), in addition to a turbocharged diesel engine and a high voltage battery. A realistic simulation model with detailed component representations will be used as a basis for deriving a hybrid model; the hybrid model will than be used for prediction in a model predictive control (MPC) strategy. Any upfront manual simplification of the simulation model is avoided to demonstrate how hybrid modeling and piecewise affine system identification techniques can be directly and systematically applied to the high fidelity industrial models.

2 Model

Our case study is an advanced 4x4 hybrid electric vehicle configuration discussed by Dextreit et al., in [1]. This vehicle is equipped with a turbocharged diesel engine, a high voltage electric battery and two electric motors one acting on the front axis and one acting on the rear axis. The front electric motor is the Crankshaft Integrated Starter Generator (CISG), which is directly mounted on the engine crankshaft and is used for starting and assisting the engine and for generating electric energy. An Electric Rear Axle Drive (ERAD) motor is located on the rear differential. The ERAD can operates as a traction motor to drive the rear wheels or as generator, either during regenerative braking or when the battery needs to be charged.

Our developments are based on a high fidelity simulation model of the overall vehicle. The simulation model is based on the nonlinear maps of the HEV components, including nonlinear models of battery and vehicle dynamics, and switching components such as gears. The simulation model can be subdivided into the following subsystems:

Electrical battery, describes the dynamics of the NiMH high voltage battery on board of the vehicle. The model equations are

$$\frac{dSoC(t)}{dt} = \frac{P_w(t)}{V_{batt}(t)} \cdot \frac{1}{C_{Ch}}, \quad V_{batt}(t) = OCV(t) - \frac{P_w(t)}{V_{batt}(t)} \cdot R(t), \qquad (1)$$

$$\frac{dOCV(t)}{dt} = \frac{P_w(t)}{V_{batt}(t)} \cdot f_1(SoC(t)) - OCV(t), \quad R(t) = f_2(SoC(t), T(t)),$$

where $0 \leq SoC \leq 1$ is the State of Charge of the battery, P_w (W) is the electrical power entering the battery, V_{batt} (V) is the output voltage, C_{Ch} (F) is the charge capacity, OCV (V) is the open circuit voltage, R (Ω) is the internal resistance, and T (°C) is the temperature. The input of (1) is the power requested ($P_w \leq 0$) or generated ($P_w \geq 0$) by the electrical motors and by the auxiliary devices. The outputs are the actual voltage V_{batt}, the delivered current $I_{batt} = \frac{P_w}{V}$, and the state of charge SoC.

Vehicle longitudinal dynamics model. The model which describes the longitudinal vehicle dynamics has the form

$$M_{tot}(t)\dot{v}_{veh}(t) = F(t), \tag{2}$$

where $M_{tot}(t)$ (kg) is the sum of the vehicle mass M and the inertial mass $M_i(t)$. Here the inertial mass is calculated as the ratio between the overall inertia at wheels $J(t)$ (kg m^2) and the square of the wheel radius r_w (m). In (2), $F(t)$ (N) is the sum of all the equivalent forces acting on the vehicle

$$F(t) = F_{drl}(t) + F_{ae}(t) + F_{rol}(t) + F_{brake}(t) + F_{gr}(t) \tag{3}$$

The forces involved in (3) are the driving force F_{drl}, which is a function of the total torque at wheels $\tau_{wheel} = \tau_{fdrl} + \tau_{\mathrm{ERAD}}$ (Nm) applied by the motors, the aerodynamic force $F_{ae}(t)$, the rolling resistance forces, $F_{rol}(t)$ and the braking force $F_{brake}(t)$ which are functions of the vehicle speed, and the force due to the gravity on a non-zero road grade, $F_{gr}(t)$. The inputs in (2), (3) are the torques applied to the wheels $\tau_{tot} = r_w \cdot F(t)$ coming from the driveline subsystem. The output is the vehicle speed v_{veh} (m/s).

Powerplant model models the internal combustion (IC) engine through different maps which characterize its instantaneous efficiency, fuel consumption, and operating limits. The inputs are the torque requested $\tau_{\mathrm{IC,req}}$ (Nm) to an existing torque controller, and the actual shaft speed ω_{shaft} (rad/s), which is also the speed of the CISG motor. We denote by J_{IC} (kg m^2) the inertia of the engine. The outputs are the torque τ_{IC} (Nm) actually delivered by the engine, and the fuel flowrate, f_{rate}.

Driveline model is composed by front and rear drivelines. The model of the front driveline includes maps representing the losses along the driveline. The rear driveline model includes maps for losses, efficiency, and limits in generating and motoring modes for the ERAD motor. The inputs are the battery states (1), the torque requested $\tau_{erad,req}$ (Nm), which is positive during the motoring and negative during the generating phase, and the torque τ_{gear} delivered to the front driveline. The outputs are the torque to each wheel and the power P_{ERAD} (W) requested or generated by the ERAD.

Transmission model includes the maps of the CISG and of the gearbox, which characterize the efficiency, the operating limits, and the transmission reductions. The main inputs are the selected gear, $gear_\sharp \in \{N, 1, 2, 3, 4, 5, 6\}$, the battery states, and the requested CISG torque $\tau_{cisg,req}$. The outputs are the transmission

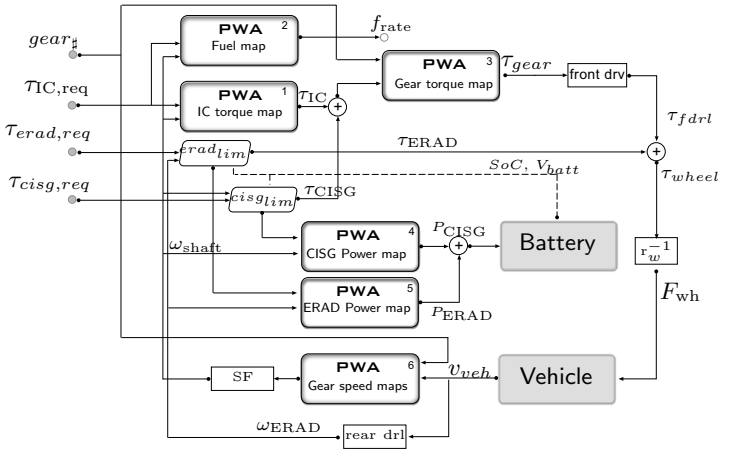

Fig. 2. Overall schematics of the HEV hybrid dynamical model

output torque τ_{gear}, the rotational speed of the gear shaft ω_{shaft}, and the power P_{CISG} (W) drained from or supplied to the battery by the CISG.

3 Hybrid Dynamical Model of the HEV

Hybrid dynamical models have been used in recent years to analyze and optimize a large variety of systems in which physical processes interact with embedded digital controllers and switching devices. Several modeling formalisms have been developed to represent hybrid systems [2,3,4], including Mixed Logical Dynamical (MLD) systems [5], which are discrete-time hybrid models useful to formulate optimization problems involving hybrid dynamics. The language HYSDEL (HYbrid Systems DEscription Language) was developed in [6] to obtain MLD models from a high level textual description of the hybrid dynamics. MLD models can be converted into piecewise affine (PWA) models [7] through automated procedures [8,9]. HYSDEL, MLD and PWA models are used in the Hybrid Toolbox for Matlab$^{\text{TM}}$ [10] for modeling, simulating, and verifying hybrid dynamical systems and for designing hybrid model predictive controllers.

The complex model described in Section 2 is approximated by a discrete-time hybrid model with sampling period $T_s = 1$s that is described in HYSDEL and automatically converted in MLD form. The procedure to obtain such a model involves the following operations:

1. *Linear identification* and time-discretization of the continuous dynamics. Sections 3.2 and 3.3 below describe the identification of discrete-time linear models of the battery (1) and of the vehicle longitudinal dynamics (2), respectively.
2. *Piecewise affine identification.* The nonlinear model is based on interconnected nonlinear maps in the form of lookup tables. These are identified

as static piecewise affine maps through the bounded-error approach [11] to hybrid system identification as detailed below in Section 3.1.

3. *Setup of the HYSDEL model.* Once each subsystem is modeled in discrete-time piecewise affine form, all the submodels are assembled and interconnected in a single HYSDEL model. This is used to generate the corresponding control-oriented MLD model and to synthesize MPC algorithms for the energy management of the HEV under consideration.

The overall hybrid dynamical system is constructed by looking at the energy distribution among the different components that constitute the HEV, rather than at the mechanical devices that compose the nonlinear simulation model, in accordance with the overall scheme depicted in Figure 2. The components of the hybrid dynamical model are described in the following section.

3.1 Piecewise Affine Identification

In order to apply linear hybrid modeling and optimization techniques, nonlinear relations between input/output variables of different subsystems must be approximated by static piecewise affine (PWA) functions. This identification task (or "hybridization" process of the model) is performed algorithmically from input/output data samples. Such samples can be either measured experimentally or obtained by evaluation of existing nonlinear models that have been previously calibrated on measured data. The identification algorithm automatically partitions the input data set into a finite number of polyhedral regions and defines a linear/affine map in each region.

In this paper we use the bounded-error approach of [11] to hybrid system identification. Consider a static PWA model in the form

$$y_k = f(\mathbf{u}_k) + \varepsilon_k, \qquad \text{where} \qquad f(\mathbf{u}_k) = \begin{cases} \theta_1' \left[\begin{smallmatrix} \mathbf{u}_k \\ 1 \end{smallmatrix} \right] & \text{if } \mathbf{u}_k \in \chi_1 \\ \vdots & \vdots \\ \theta_s' \left[\begin{smallmatrix} \mathbf{u}_k \\ 1 \end{smallmatrix} \right] & \text{if } \mathbf{u}_k \in \chi_s, \end{cases} \tag{4}$$

where $\mathbf{u}_k \in \mathbb{R}^n$ are the input samples, $y_k \in \mathbb{R}$ are the corresponding output samples, $\varepsilon_k \in \mathbb{R}$ are the error terms, $k = 1, \ldots, N$. $\chi_i = \{\mathbf{x} : H_i \mathbf{u}_k \leq K_i\}$, are polyhedral sets defining a partition of the given set of interest $\chi \subseteq \mathbb{R}^n$, and $\theta_i \in \mathbb{R}^{n+1}$, $i = 1, ..., s$, are the parameter vectors defining the affine submodels.

Given the tolerated bound $\delta > 0$ on the fit error ε_k, the bounded-error approach determines a PWA model (4) satisfying the condition $|y_k - f(\mathbf{u}_k)| \leq \delta$. The bound δ is the tuning knob of the procedure. It determines the tradeoff between complexity and accuracy of the model to fit samples. In this paper we have modified the toolbox of [12] to approximate PWA functions based on a maximum "relative" error $\delta_{rel} > 0$

$$\frac{|y_k - f(\mathbf{u}_k)|}{1 + |y_k|} \leq \delta_{rel} \ , \quad \forall k = 1, \ldots, N. \tag{5}$$

Compared to the original absolute error proposed in [11], we have found that the criterion (5) leads to a reduced complexity in terms of number s of affine models.

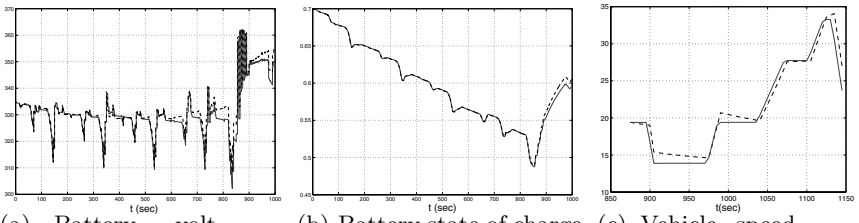

(a) Battery voltage dynamics V_{batt} (dashed: linear model, solid: nonlinear model)

(b) Battery state of charge dynamics (dashed: linear model, solid: nonlinear model)

(c) Vehicle speed dynamics (dashed: linear model, solid: nonlinear model)

Fig. 3. Open-loop validation of the linear ARX model of the battery and of the vehicle chassis model

Given N data points $(y_k, \mathbf{u}_k)$, $k = 1, \ldots, N$ and a chosen $\delta_{rel} > 0$, the three-step procedure proposed in [11] is applied to look for the minimum positive integer s, for a partition $\chi_1, \ldots, \chi_s$, and for a set of parameter vectors $\theta_1, \ldots, \theta_s$ such that the corresponding PWA model (4) satisfies the bounded error condition (5). As detailed in the next sections, different parameters δ_{rel} were optimized for each identified map, depending on the relevance of the fit error on the dynamic behavior of the overall hybrid system. The N data points for each PWA model are chosen using the response of the nonlinear model controlled by a rule-based controller developed in [1] and a collection of points uniformly distributed on the input range of the nonlinear map. The toolbox of [12] has also been interfaced to the Hybrid Toolbox [10] by automatically generating the HYSDEL code that describes the identified PWA function.

3.2 Battery Model

In order to model the battery described by the nonlinear dynamics (1) in a hybrid form oriented toward the synthesis of MPC controller, the model was approximated as a piecewise affine autoregressive exogenous (PWARX) model via the parametric identification procedure [11].

By restricting the safe range of the State of Charge, $SoC \in [0.2, 0.8]$, neglecting the dependence on temperature (we assumed $T = 25°C$ constant) and assuming that the charging and discharging characteristics are equal, a satisfactory fit has been obtained by a multi-output PWA autoregressive model that consists of only one partition, that is, by the linear autoregressive model

$$\begin{bmatrix} SoC(k) \\ V_{batt}(k) \end{bmatrix} = b_0 P_w(k) + b_1 P_w(k-1) + a_{1s} SoC(k-1) + a_{2s} SoC(k-2) + a_{1v} V_{batt}(k-1) + a_{2v} V_{batt}(k-2) \quad (6)$$

where k denotes the sampling instant for sampling period $T_s = 1$s, a_{1s}, a_{2s}, b_0, b_1, a_{1v}, $a_{2v} \in \mathbb{R}^2$ are the coefficient matrices. The model was validated against the response of the nonlinear model using $N_v = 1000$ samples of a real use of the

battery during a driving cycle. The results of the comparison, obtained using open-loop simulation, are reported in Figure 3. The fit on validation data is $\simeq 96\%$ for the SoC and $\simeq 77\%$ for V_{batt}.

In order to account for modeling errors, the State of Charge constraints enforced by the controller are set tighter than real safety and realistic limits

$$0.3 \leq SoC(t) \leq 0.7, \ \forall t \geq 0. \tag{7}$$

Since in fact the real SoC safe range is is wider, this constraint is treated as soft, i.e., its violations will cause an increased value of the cost, which means that they are tolerable, but only during short transients.

3.3 Vehicle Model

For the purpose of power management only the force F_{drl} delivered by the controlled motors to the driveline, $F_{drl} \geq 0$, is considered as a manipulated input to the linear model (2) of the vehicle longitudinal dynamics. The remaining forces $F_{ae}(t)$, $F_{rol}(t)$, $F_{gr}(t)$ model resistance effects on the car. The braking force F_{brake} is considered as a disturbance, since it is actuated by the driver. The full nonlinear model of the vehicle longitudinal dynamics takes into account the fact that the equivalent inertia of the system is not constant and in particular it depends on the engaged gear. Nonetheless, the simple mass-damper model

$$M\dot{v}_{veh} + \beta v_{veh} = \frac{1}{r_w} \cdot \tau_{\text{wh}} \tag{8}$$

was fit to N simulation data of wheel torque τ_{wh}, speed v_{veh}, and acceleration $\dot{v}_{veh}$ obtaining a good approximation. The parameters M and β were simply estimated by solving the standard least square estimation problem

$$\left[\begin{smallmatrix} M \\ \beta \end{smallmatrix}\right] = (X^T X)^{-1} X^T Y, \ X = \begin{bmatrix} \dot{v}(0) & v(0) \\ \vdots & \vdots \\ \dot{v}(N-1) & v(N-1) \end{bmatrix}, \ Y = \frac{1}{r_w} \begin{bmatrix} \tau(0) \\ \vdots \\ \tau(N-1) \end{bmatrix}. \tag{9}$$

Figure 3(c) compares the vehicle speed signal generated by the open-loop simulation of the estimated linear model excited by τ_{wh} against the vehicle speed signal obtained by simulating the full nonlinear model. The open-loop simulation error over a period of 300 s is bounded and does not tend to diverge; it is smaller than 2 m/s for the most part of the simulation.

3.4 Internal Combustion Engine

Since the aim of the hybrid dynamical model is to synthesize a control algorithm for managing power flows within HEV, the engine and its low-level torque regulator are modeled as a subsystem whose inputs are the desired torque $\tau_{\text{IC,req}}$ to the crankshaft and engine speed ω_{shaft}, and whose outputs are the actual delivered torque τ_{IC} and the fuel flowrate f_{rate}, therefore assuming torque generation dynamics are fast enough to be negligible. This assumption is justified by the

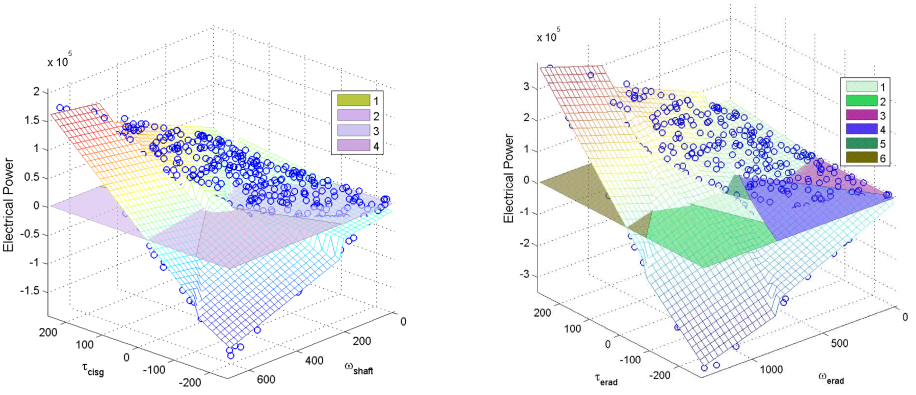

(a) CISG electrical motor (b) ERAD electrical motor

Fig. 4. PWA maps of the electric motors

fact that energy management is performed at a much slower rate than torque control. Accordingly, two of the following PWA output maps were identified

$$\tau_{\mathrm{IC,req}} - \tau_{\mathrm{IC}} = f_{PWA,\tau}(\tau_{\mathrm{IC,req}}, \omega_{\mathrm{shaft}}), \tag{10}$$

which consists of 4 regions, with a fit error below 10%, and

$$f_{\mathrm{rate}} = f_{PWA,f}(\tau_{\mathrm{IC,req}}, \omega_{\mathrm{shaft}}), \tag{11}$$

which consists of 5 regions, with a fit below 5%.

3.5 Electric Motors

The electric motors are assumed to have fast dynamics and generate torque equal to the requested torque unless limits are exceeded by the requested torque, in which case the actual torque is saturated. The limits are not modeled in the hybrid model, but rather calculated and imposed by the MPC controller externally through a piecewise affine bound. The elimination of the limit maps from the model is justified by the fact that the saturation limits are never reached in simulation as long as the constraints on the State of Charge SoC of the battery are enforced, and this reduces the complexity of the hybrid dynamical model. The mechanical power delivered by the CISG and ERAD motors are $P_{\mathrm{CISG,mec}} = \tau_{\mathrm{CISG}} \cdot \omega_{\mathrm{shaft}}$ and $P_{\mathrm{ERAD,mec}} = \tau_{\mathrm{ERAD}} \cdot \omega_{\mathrm{ERAD}}$, respectively. The following PWA maps represent the actual delivered electrical power $P_{\mathrm{CISG,ele}}$ and $P_{\mathrm{ERAD,ele}}$

$$P_{\mathrm{CISG,ele}} = f_{PWA,c}(\tau_{\mathrm{CISG}}, \omega_{\mathrm{shaft}}), \;\; P_{\mathrm{ERAD,ele}} = f_{PWA,e}(\tau_{\mathrm{ERAD}}, \omega_{\mathrm{ERAD}}). \tag{12}$$

The functional relationships in (12) have been identified from the full nonlinear model and are reported in Figure 3.4. The maps (12) incorporate the effect of electro-mechanical losses.

Table 1. Elecrical Motor PWA maps limits

	max speed (rad/s)	torque range (Nm)	max power loss (kW)
CISG	700	-200 ÷ 200	13
ERAD	1300	-300 ÷ 300	21

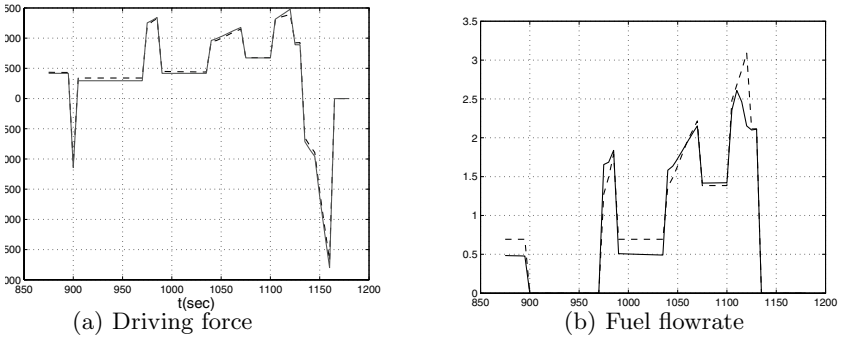

(a) Driving force (b) Fuel flowrate

Fig. 5. Open-loop validation of the IC engine model: PWA model (dashed), nonlinear model (solid)

The ERAD motor operates in a wider range than the CISG motor (see Table 1). The latter mainly assists the IC engine. A reasonable tradeoff between accuracy of the maps and model complexity has been reached by setting a relative maximum fitting error of 15% in the PWA identification algorithm for both maps. The number of regions for the ERAD and CISG electrical power maps is 6 and 4, respectively.

3.6 Gear Model

The model of the gearbox is split in two different maps. As sketched in Figure 2 the PWA map of gear torque models the effects of the mechanical reduction on the torque entering the gearbox, $\tau_{\text{ingear}} = \tau_{\text{IC}} + \tau_{\text{CISG}}$ [Nm], as a function of the selected gear, $gear_\sharp$,

$$\tau_{gear} = f_{PWA}(\tau_{\text{ingear}}, gear_\sharp). \tag{13}$$

A second one-dimensional map defines the transmission ratio $TR_\sharp$ for each gear, where $\sharp$ denotes gear number. The transmission ratio relates the shaft speed ω_{shaft} [rad/s] and the actual vehicle speed v_{veh} [m/s]

$$\omega_{\text{shaft}} = v_{veh} \cdot TR_\sharp \cdot SF, \tag{14}$$

where SF is the scaling factor due to the front differential.

3.7 Overall Hybrid Dynamical Model

The overall hybrid dynamical model is constructed according to the structure depicted in Figure 2, where each component has been approximated through linear or piecewise affine identification as described in the previous sections. The model has been validated by running an open-loop simulation on the New European Driving Cycle (NEDC), which defines a vehicle speed reference profile, $v_{veh,ref}$, to be tracked for a duration of 20 minutes, along with the gear to engage. Figure 5(a) reports the traction force acting on the vehicle, Figure 5(b) the fuel flowrate consumed by the vehicle. The quality of the fit is considered adequate, as the mere role of the model is to predict the behavior of the HEV over a short time horizon as required for model predictive control.

In order to track the vehicle speed with zero steady-state offset the model is extended by introducing integral action. The sampled desired vehicle speed $v_{veh,ref}$ and the integral $I_{v,err}$ of the difference between $v_{veh,ref}$ and v_{veh} are included as additional states

$$\begin{aligned} v_{veh,ref}(k+1) &= v_{veh,ref}(k) \\ I_{v,err}(k+1) &= I_{v,err}(k) + T_s(v_{veh}(k) - v_{veh,ref}(k)) \end{aligned}$$

where $T_s = 1$s is the sampling period. With the aim of reducing the prediction horizon of the hybrid MPC controller based on the hybrid dynamical model developed above, rather than considering the tracking error of the state of charge we consider its one step ahead prediction, obtained by iterating (6) for one step under the assumption that the electrical power satisfies $P_w(k+1) = P_w(k)$.

The braking force F_{brake} from the driver is also modeled as a constant state $F_{brake}(k+1) = F_{brake}(k)$, although it will be assumed to be unknown in the following simulations by the controller, and hence set $F_{brake} = 0$.

The overall hybrid dynamical model has been described in HYSDEL and converted to MLD form using the Hybrid Toolbox for Matlab [10]. The resulting MLD model has 9 continuous states ($v_{veh}(k)$, $I_{v,err}(k)$, $v_{veh,ref}(k)$, $SoC(k)$, $SoC(k-1)$, $V_{batt}(k)$, $V_{batt}(k-1)$, $P_w(k-1)$, $F_{brake}(k)$), 7 binary states storing the current engaged gear (Neutral, 1st, ..., 6th) and subject to an exclusive-or constraint, 3 continuous inputs ($\tau_{\mathrm{IC,req}}$, $\tau_{ERAD,req}$, $\tau_{CISG,req}$), 32 binary inputs used to detect the active regions in the 6 PWA maps (for each map the corresponding group of binary inputs is subject to an exclusive-or constraint), 56 continuous auxiliary variables, used for representing the PWA maps, engine speed, engine torque, and other ancillary variables, 1 continuous output, fuel consumption f_{rate}, no binary auxiliary variables, and 490 mixed-integer inequalities.

4 Model Predictive Control Design

MPC was used in many industrial applications [13], and more recently model predictive control of hybrid dynamical systems has shown potential for applications in the automotive domain [14,15,16,17,18,19]. In this section we design an MPC controller for the HEV based on the overall hybrid dynamical model

described in Section 3. In the MPC approach, at each sampling instant a finite horizon open-loop optimization problem is solved, using the current state as the initial condition of the problem. The optimization provides a control sequence, only the first element of which is applied to the process. This process is iteratively repeated at each subsequent time instant, thereby providing a feedback mechanism for disturbance rejection and reference tracking. The optimal control problem is defined as:

$$\min_{\xi} J(\xi, x(t)) \triangleq Q_\rho \rho^2 + \sum_{k=1}^{N} (\Gamma_x x_k - x_{ref})^T S (\Gamma_x x_k - x_{ref}) + \tag{15a}$$
$$+ \sum_{k=0}^{N-1} (\Gamma_u u_k - u_{ref})^T R (\Gamma_u u_k - u_{ref}) + (y_k - y_{ref})^T Q (y_k - y_{ref}),$$

$$\text{subj. to} \begin{cases} x_0 & = x(t), \\ x_{k+1} & = Ax_k + B_1 u_k + B_3 z_k, \\ y_k & = Cx_k + D_1 u_k + D_3 z_k, \\ E_3 z_k & \leq E_1 u_k + E_4 x_k + E_5, \\ 0.3 - \rho \leq SoC_k & \leq 0.7 + \rho, \end{cases} \tag{15b}$$

where N is the control horizon, $x(t)$ is the state of the MLD system at sampling time t, $\xi \triangleq [u_0^T, z_0^T, \ldots, u_{N-1}^T, z_{N-1}^T, \rho]^T \in \mathbb{R}^{59N+1} \times \{0,1\}^{32N}$ is the optimization vector, Q, R and S are weight matrices, Q_ρ is a large weight used to enforce the softened version (15b) of constraint (7), and $\Gamma_u \in \mathbb{R}^{3\times 36}$, $\Gamma_x \in \mathbb{R}^{3\times 16}$ are matrices that select the subset of vector components to be weighted (Γ_u, Γ_x are formed by rows of identity matrices). In particular we define the reference signals used in (15) for the output and for the components selected by Γ_u, Γ_x as

$$y_{ref} \triangleq f_{\text{rate,ref}}, \tag{16a}$$
$$u_{ref} \triangleq [\tau_{\text{IC,req}} \ \tau_{\text{ERAD,req}} \ \tau_{\text{CISG,req}}]', \tag{16b}$$
$$x_{ref} \triangleq [v_{\text{veh,ref}} \ \ I_{\text{v,err}} \ \ SoC_{\text{ref}}]', \tag{16c}$$

and, accordingly, we set the cost weights in (15b) to be

$$Q = q_{\text{fuel}}, \quad R = \begin{bmatrix} r_{\tau,\text{IC}} & 0 & 0 \\ 0 & r_{\tau,\text{CISG}} & 0 \\ 0 & 0 & r_{\tau,\text{ERAD}} \end{bmatrix}, \quad S = \begin{bmatrix} s_{\text{v,veh}} & 0 & 0 \\ 0 & s_{\text{SoC}} & 0 \\ 0 & 0 & s_{\text{v,int}} \end{bmatrix}, \ Q_\rho = 10^5,$$

where the components of vector u_{ref} are all zero in order to minimize the control action.

Problem (15) can be transformed into a mixed integer quadratic program (MIQP), i.e., into the minimization of a quadratic cost function subject to linear constraints, where some of the variables are binary. Even if this class of problems has exponential complexity, efficient numerical tools for its solution are available [20].

5 Simulation Results

The closed-loop behavior of the HEV in closed loop with MPC controller has been evaluated in simulations by using the high-fidelity nonlinear model described in Section 2. The design parameters for the MPC (15) are the prediction

Table 2. MPC design parameters ($r_{\tau,\mathrm{IC}} = 6{\cdot}10^{-2}$, $r_{\tau,\mathrm{CISG}} = 3{\cdot}10^{-2}$, $r_{\tau,\mathrm{ERAD}} = 3{\cdot}10^{-2}$, $s_{\mathrm{v,veh}} = 5{\cdot}10^{3}$). The number in the first column represents the MPC design number (0 = conventional vehicle). The fuel consumption values are normalized to the conventional vehicle consumption.

	q_{fuel}	s_{SoC}	$s_{\mathrm{v,int}}$	fuel cons (norm)	$\max \lvert v_{veh} - v_{veh,ref} \rvert$	$\max \lvert SoC - SoC_{ref} \rvert$
0	*	*	*	1	*	*
1	1e-2	2e6	10	0.79	2.105	0.1364
2	1e1	1e6	1	0.76	2.789	0.2484

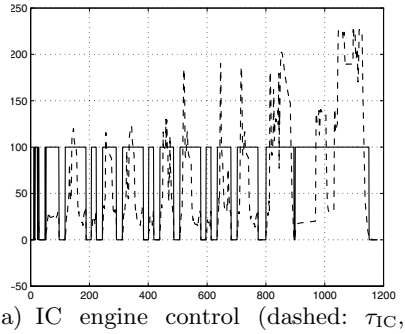

(a) IC engine control (dashed: τ_{IC}, solid: IC engine on/off signal)

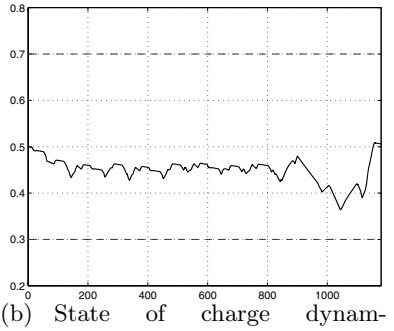

(b) State of charge dynamics(dashed: SoC bounds, solid: SoC dynamics)

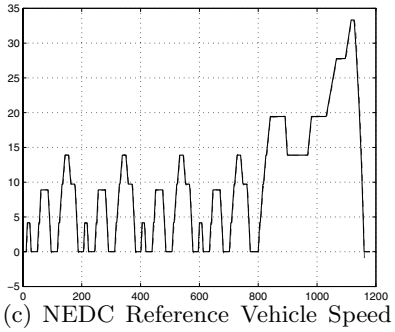

(c) NEDC Reference Vehicle Speed profile

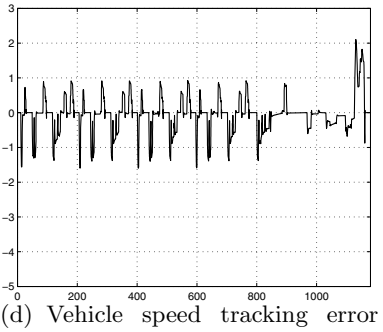

(d) Vehicle speed tracking error ($v_{\mathrm{veh}} - v_{\mathrm{veh,ref}}$)

Fig. 6. MPC design #1: closed-loop response

horizon $N = 1$, and weights $r_{\tau,\mathrm{IC}} = 6{\cdot}10^{-2}$, $r_{\tau,\mathrm{CISG}} = 3{\cdot}10^{-2}$, $r_{\tau,\mathrm{ERAD}} = 3{\cdot}10^{-2}$, $s_{\mathrm{v,veh}} = 5 \cdot 10^{3}$. The weights q_{fuel}, s_{SoC} and $s_{\mathrm{v,int}}$ are reported in Table 2 for two different MPC designs. Note that the weight on $r_{\tau,\mathrm{IC}}$ is much greater than $r_{\tau,\mathrm{CISG}}$, $r_{\tau,\mathrm{ERAD}}$ to force the use of torque from electric motors rather than from the IC engine, and that $s_{\mathrm{v,int}}$ is used to maintain the speed tracking performance.

For both controllers it took approximately 175.5 s to simulate the closed-loop system on a PC Intel Centrino Duo 2.0 GHz with 2GB RAM running the Hybrid Toolbox for Matlab [10] and the MIQP solver of CPLEX 9 [20], of which 156.7 s

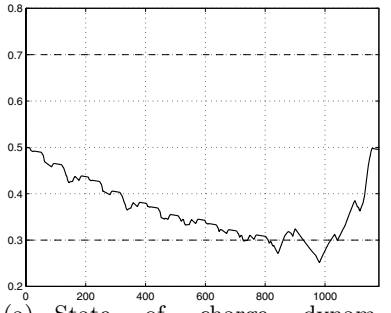

(a) State of charge dynamics(dashed: SoC bounds, solid: SoC dynamics)

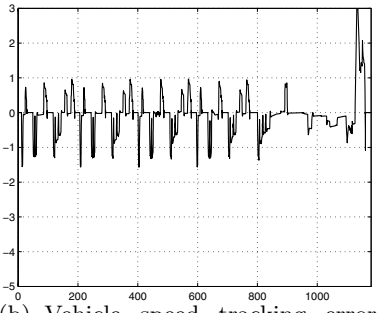

(b) Vehicle speed tracking error ($v_{\text{veh}} - v_{\text{veh,ref}}$)

Fig. 7. MPC design #2: closed-loop response

are spent by CPLEX, that is an average of approximately 0.13 s per time step. The control action is computed in the worst case in approximately 0.29 s. The closed-loop dynamics obtained from the first MPC design are described in Figure 6.

In this simulation q_{fuel} has a small weight as the fuel consumption is less important than keeping the battery SoC close to the setpoint. To improve fuel consumption the internal combustion engine is turned off when the torque request is lower than a given threshold, see Figure (6(a)). The results of the second MPC design are shown in Figure 7, where a higher emphasis to fuel consumption is given, where more freedom to draw power from the battery (lower s_{SoC}) is allowed to the controller, which also has a lower weight on the speed tracking integral action ($s_{\text{v,int}}$). The weight on $s_{\text{v,veh}}$ allowed to maintain the maximum error in speed tracking smaller than 3.2 [m/s]. The SoC signal violates the soft constraint (15b) on minimum charge for a maximum time of 92s. However, it should be noted that the SoC always remains in the physical battery safety and reliability range $SoC \in [0.2, 0.8]$. For both MPC designs the fuel consumption is reduced with respect to a conventional vehicle. In the first simulation the fuel consumption improvement is 20.7%. In the second simulation the controller is allowed to use more electric power due to smaller weight on s_{SoC}, and this results a slight violation of the soft constraint. On the other hand the fuel consumption improvement is 23.8%. These improvements are similar to the values reported in [1], but it is interesting to observe that in this paper the MPC controller does not exploit any knowledge of the driving cycle but only of the vehicle model.

6 Conclusions

In the paper we have exemplified an effective control approach for advanced powertrain systems which combines hybrid modeling, identification and model predictive control. In this approach, piecewise affine system identification techniques serve as a bridge between detailed nonlinear simulation models (or experimental

powertrain hardware) and hybrid models in such a way that the on-line implementation of model predictive control becomes feasible using a mixed integer quadratic programming. In the paper, a realistic (industrial strength) simulation model with high fidelity components representation was used as a basis for deriving an approximate hybrid model: the latter was used to define the hybrid MPC optimization problem. This design approach could have been equally applied to experimental vehicle data or to a mixture of experimental data and simulation data.

References

1. Dextreit, C., Assadian, F., Kolmanovsky, I.V., Mahtani, J., Burnham, K.: Hybrid electric vehicle energy management using game theory. In: Proceedings of SAE World Congress, Detroit, MI (April 2008)
2. Branicky, M.S.: Studies in hybrid systems: modeling, analysis, and control. PhD thesis, LIDS-TH 2304, Massachusetts Institute of Technology, Cambridge, MA (1995)
3. Heemels, W.P.M.H., De Schutter, B., Bemporad, A.: Equivalence of hybrid dynamical models. Automatica 37(7), 1085–1091 (2001)
4. Lygeros, J., Johansson, K.H., Simic, S.N., Zhang, J., Sastry, S.S.: Dynamical properties of hybrid automata. IEEE Trans. Automatic Control 48, 2–17 (2003)
5. Bemporad, A., Morari, M.: Control of systems integrating logic, dynamics, and constraints. Automatica 35(3), 407–427 (1999)
6. Torrisi, F.D., Bemporad, A.: HYSDEL — A tool for generating computational hybrid models. IEEE Trans. Contr. Systems Technology 12(2), 235–249 (2004)
7. Sontag, E.D.: Nonlinear regulation: The piecewise linear approach. IEEE Trans. Automatic Control 26(2), 346–358 (1981)
8. Bemporad, A.: Efficient conversion of mixed logical dynamical systems into an equivalent piecewise affine form. IEEE Trans. Automatic Control 49(5), 832–838 (2004)
9. Geyer, T., Torrisi, F.D., Morari, M.: Efficient Mode Enumeration of Compositional Hybrid Models. In: Maler, O., Pnueli, A. (eds.) HSCC 2003. LNCS, vol. 2623, pp. 216–232. Springer, Heidelberg (2003)
10. Bemporad, A.: Hybrid Toolbox – User's Guide (January 2004), `http://www.dii.unisi.it/hybrid/toolbox`
11. Bemporad, A., Garulli, A., Paoletti, S., Vicino, A.: A bounded-error approach to piecewise affine system identification. IEEE Trans. Automatic Control 50(10), 1567–1580 (2005)
12. Paoletti, S., Roll, J.: PWAID: Piecewise affine system identification toolbox (2007)
13. Qin, S.J., Badgwell, T.A.: A survey of industrial model predictive control technology. Control Engineering Practice 11(7), 733–764 (2003)
14. Borrelli, F., Bemporad, A., Fodor, M., Hrovat, D.: An MPC/hybrid system approach to traction control. IEEE Trans. Contr. Systems Technology 14(3), 541–552 (2006)
15. Giorgetti, N., Ripaccioli, G., Bemporad, A., Kolmanovsky, I.V., Hrovat, D.: Hybrid Model Predictive Control of Direct Injection Stratified Charge Engines. IEEE/ASME Transactions on Mechatronics 11(5), 499–506 (2006)

16. Di Cairano, S., Bemporad, A., Kolmanovsky, I., Hrovat, D.: Model predictive control of magnetically actuated mass spring dampers for automotive applications. Int. J. Control 80(11), 1701–1716 (2007)
17. Vašak, M., Baotić, M., Morari, M., Petrović, I., Perić, N.: Constrained optimal control of an electronic throttle. Int. J. Control 79(5), 465–478 (2006)
18. Corona, D., De Schutter, B.: Adaptive cruise control for a smart car: A comparison benchmark for MPC-PWA control methods. IEEE Trans. Contr. Systems Technology 16(2), 365–372 (2008)
19. Ortner, P., del Re, L.: Predictive control of a diesel engine air path. IEEE Trans. Contr. Systems Technology 15(3), 449–456 (2007)
20. ILOG, Inc. CPLEX 9.0 User Manual. Gentilly Cedex, France (2003)